Low Dose Ionizing Radiation Effects on Dielectric Relaxation Dynamics and Structural Erosion in Testis of Albino Rat

M.S. Orkaa[1 *], A. A. Bello[2], J. Z. Dlama[3], A. M. Hamza[2], J. U. Ewuga[4]

[1]Department of Radiography and Radiation Science, Rev Fr Moses Orshio Adasu University, Makurdi, Nigeria.

[2]Department of Physics, Federal University of Lafia, Nigeria

[3]Department of Radiography and Radiation Science, Federal University of Lafia, Nigeria

[4]Department of Physics, Karl Kum University, Vom, Nigeria.

[*]Corresponding Author

DOI: https://doi.org/10.51584/IJRIAS.2026.11100057

Received: 17 October 2026; Accepted: 22 October 2026; Published: 04 November 2026

ABSTRACT

The present work examines the biophysical effects of low-dose X-ray radiation on healthy albino rat testis tissues to correlate macro structural degradation with micro-level soft-tissue electrical property alterations. Irradiating male albino rats with whole-body X-rays (0-5.25 mGy). To evaluate dielectric permittivity (ε`) and electrical conductivity (σ) of excised testis tissue, a bespoke parallel plate sample cell was used at 37 °C. A digital capacitance meter, signal generator, and conductometer were used. SEM imaging visualized morphological changes. COMSOL Multiphysics 5.5's 2D axisymmetric model simulated radiation transport and localized energy deposition. Non-linear, threshold-dependent soft tissue dielectric profile degradation was observed. Control tissues exhibited healthy Maxwell-Wagner interfacial polarization, with ε′ greatly decreasing from 5952.4 at 0.1 kHz to 12.2 at 20 kHz. At low doses (0 to 0.67 mGy), tissues changed gradually, but at 1.35 mGy, biophysical collapse occurred. In the critical zone, dielectric strength (Δ) decreased from 15.94 to 8.42 and relaxation time (τ) decreased from 47 to 25 µs. However, the low-frequency conductivity (σ) at 0.1 kHz increased from 7.65 S/m (control) to 7.70 S/m at the highest dose of 5.25 mGy. SEM research confirmed that 5.25 mGy exposure produced basement membrane collapse, resulting in dense and cohesive cell masses breaking up into an eroded, porous honeycomb sponge. COMSOL simulations showed an exponential decrease with travel length and a maximum of absorbed dosage at about the entrance surface (1 to 3 mm). Low-dose X-ray damage disrupted the normal cell borders, reduced the charge storage capacity and increased the low-frequency electrical conductivity of the testes. Developed quadratic formulas precisely model the tissue-field dynamics and enable the development of advanced bio impedance algorithms for targeted clinical oncology therapy and radiological safety processes.

Keywords: X-ray, Tissue, low-dose

INTRODUCTION

Radiobiology is concerned with the effects of low-level ionizing radiation on biology. This is vital to understanding environmental safety and risks to human health. At the cellular level, the first signs of damage are usually observed when radiation interacts with biological tissues. Cells may collapse or fail to function (Wei et al., 2026). Traditional techniques such as scanning electron microscopy (SEM) are excellent for temporally observing cell degradation, but do not show changes as they occur [6][11]. And that's why scientists are now studying the low-frequency dielectric properties of tissues. The method is new and does not damage tissues and therefore is a promising tool in medical diagnostics and radiobiology [4]. The low

ISSN No. 2321-2705 | DOI: 10.51244/IJRSI |Volume XIII Issue X October 2026

frequency α-dispersion region, between 20 Hz and 20 kHz, is of interest. It all depends on the way ions move and on the way interfaces at cell membranes polarize [13, 10]. This means that researchers need to connect hands-on bioimpedance studies with computer models to see these tiny changes in real-time. [1] Radiation transport and interaction with tissue can be simulated using tools like COMSOL Multiphysics.

To go deep into these changes caused by radiation, scientists need to use modern methods taking into account the latest findings on the interaction of tissues with fields [9]. Much progress has been made in the knowledge about the way high energy radiations damage tissues in the last decade. It breaks down tissue boundaries, impairs their electrical charge-holding capacity and creates better conducting pathways for electricity. In the present study, these issues are investigated by analyzing the testis tissue of albino rats exposed to low doses of X-rays. This paper presents a combination of physical capacitance and conductivity measurements, mathematical modelling, SEM ultrastructural analysis, and 2D axisymmetric simulations with COMSOL, for the degradation of biological structures under radiation. These quantitative models help predict electromagnetic properties of tissues, which is crucial for developing better bioimpedance algorithms for clinical radiotherapy and protecting against radiation.

METHODOLOGY

A special container called a parallel plate sample cell was made from a plastic syringe of Perspex material. This was done by following the steps outlined by [14]. The container made had two electrodes that were 3.2 cm apart. The inside of the syringe was about 0.947 cm across, which allowed for a change in the distance between the electrodes to 3.2 cm. This sample cell was also connected to several different devices: a STEREN Digital capacitance meter, a JDS66 DDS signal generator and a TH 27 conductometer. The devices were used to measure the ability of biological samples to conduct electricity and store energy at different frequencies. The capacitance meter is easy to use for taking measurements, as it has clip test leads that connect to the sample cell. The combination of these devices allowed to deduce a better understanding of the behavior of the samples under different conditions. To determine the relative permittivity, the equation below was used;

$$C = \varepsilon_0 \varepsilon_r {}^{A}/_{d} \qquad 1$$

Where C is the capacitance of the parallel plate capacitor in Farad, ε_0 ($8.85\text{x}10^{-12}$ F/m) is the permittivity of free space, ε_r is the relative permittivity of the material under test, A is the surface area of the plates in square meters, and d is the distance between the plates in meters.

Also, to determine the dielectric loss factor ε'' the equation below was used;

$$\sigma = 2\pi f \varepsilon_0 \varepsilon'' \qquad 2$$

Where σ is the conductivity of the material in S/m, ε_0 ($8.85\text{x}10^{-12}$ F/m) is the permittivity of free space, ε'' is the dielectric loss factor of the material, and f is the frequency.

A total number of 6 male albino rats were used for this research, with each rat weighing between 185 to 200 grams. Out of the six (6) rats, one was used as control experiment while the rest five (5) were irradiated with varying x-rays dose. The machine used was an XD4-2.9/100 mobile X-ray generator and was used at specific levels - between 65 and 95 kV and 32 mA. The X-ray was filtered using a 2.9 mm aluminium filter. The distance between the X-ray source and the rat skin was kept at 40 cm. Using a process known as collimation, the size of the X-ray field was adjusted so that the whole body of the rat was covered.

In order to calibrate, thermoluminescent dosimeter chips were used. These chips were then placed under the skin of the rats at the abdominal area, near the stomach, to measure the amount of radiation in different organs of the rat (specifically the testis). After the rats were exposed to radiation, the chips were taken out, put in special containers to keep them dark, and sent off to be read. This helped the researchers get accurate measurements of the radiation doses in concerned part of interest of the rats' bodies.

ISSN No. 2321-2705 | DOI: 10.51244/IJRSI |Volume XIII Issue X October 2026

Rats that had been exposed to radiation, were observed and then excised after 2 hours of exposure. Tissue sample from the testis of these rats were taken and its electrical properties measured at a temperature of 37 °C. To keep everything clean, samples were stored in a special sealed container during the measurements. Also, repeated measurements were taken to ensure accurate results.

SEM Analysis

After dielectric measurements were taken and recorded, moisture was further removed from the samples to avoid collapse of the tissues. Then the tissues were sliced into very thin slices so they were easier to image. Samples were analyzed with a scanning electron microscope, a powerful instrument that allowed researchers to see the way radiation had changed their shape and structure. The high-tech imaging was carried out at the Nigerian Building and Road Research Institute in Abuja using a top-notch machine known as the Zeiss Gemini 1-Sigma 300. This gave a very detailed picture of the effects of radiation on the tissues.

Model for X-ray Beam Propagation in Tissue

COMSOL Multiphysics software, version 5.5, was used to simulate the absorption of X-rays in biological tissues. Here X-ray absorption simulation involves tracking high energy radiation as it passes through a material and loses energy. This is based on the Beer-Lambert law.

A three-dimensional computational model was developed to evaluate the spatial distribution and depth penetration of the X-ray beam based on a 2D axisymmetric formulation in the COMSOL Multiphysics software environment. This geometric optimization exploits angular symmetry to greatly reduce the computational overhead while preserving the spatial accuracy along the main axis of propagation (z-axis). The basic material properties were; absorption coefficient, electrical conductivity, and relative permittivity. The target geometry was modelled by a thick cylindrical phantom representing multi-layered biological domains. The boundary system has orthogonal triad (t_1, t_2, n) which emanates from deformed configuration frame setting. The spatial global Cartesian (z-axis) is where the first tangent direction is created from. A discrete range of photon energies, E, was swept parametrically for the simulation of a monochromatic spectrum. The material characteristics were made energy dependent by linear interpolation of experimental mass attenuation coefficients (μ/ρ) over the varying incident spectrum. The intensity of the incident X-ray beam (I_0) was discretely defined by the structured indexing system assigned to the two main biological tissue components under study.
Inside the phantom, the material transitions and structural boundaries were handled dynamically using a switch expression, allowing for smooth spatial segmentation. Radiation transport and subsequent energy deposition were governed by the underlying mathematical physics domain. This mapped the localized absorbed dose (D, in j/kg) through the geometry. Once the parametric sweep was executed, post-processing and visualization of the resulting attenuating profiles and depth-dose distributions along the central axis of propagation were performed.

RESULTS

Table 1 Values of Dielectric Permittivity, ε′ For X-Irradiated and Non-Irradiated (Control) Healthy Rats' Testis Tissues at Selected Frequencies

F kHz Dose mGy	0.02	0.1	0.3	0.6	0.8	1	2	5	8	10	15	20
0 (control)	30.1	5952.4	-	955.3	709.1	562.4	268.0	94.8	51.7	37.4	18.2	12.2
0.15	27.2	5376.4	1763.8	862.8	640.5	507.9	242.1	85.6	46.7	33.7	16.4	10.4
0.67	25.8	5088.4	1669.3	816.6	606.2	480.8	229.1	81.0	44.2	31.9	15.6	9.8
1.35	13.6	2688.2	881.9	431.4	320.3	253.9	121.1	42.8	23.3	16.9	8.2	5.2
2.50	10.7	2112.2	692.9	388.9	251.6	199.6	95.1	33.6	18.3	13.3	6.5	4.1
5.25	6.8	1143.8	338.2	189.6	987.2	101.2	69.8	22.8	12.4	6.1	4.2	1.8

Table 1 shows that un-irradiated tissue exhibits classic dielectric dispersion behavior [7] with extreme ε' values (5952.4 at 0.1 kHz vs 12.2 at 20 kHz) and a steep ε' decrease which is characteristic of Maxwell-

ISSN No. 2321-2705 | DOI: 10.51244/IJRSI |Volume XIII Issue X October 2026

Wagner interfacial polarization. All doses present significant changes in ε′ with different patterns; at 0.15 mGy, there is a moderate decrease at 0.1 kHz and at 5.25 mGy, there is a severe decrease at 0.1 kHz with a maximum and minimum frequency dependent sensitivity effect at 0.1 kHz and 20 kHz respectively.

Table 2 Values for Conductivity, σ (S/m) for X-Irradiated and Non-Irradiated (Control) Healthy Rats' Testis Tissues at Selected Frequencies.

F (kHz) Dose (mGy)	0.02	0.1	0.3	0.6	0.8	1	2	5	8	10	15	20
0 (control)	6.8	7.65	-	7.05	7.0	6.95	6.7	5.9	4.45	3.65	3.6	-
0.15	6.8	7.6	-	7.0	6.95	6.80	6.7	5.70	4.40	3.62	3.60	4.0
0.67	6.85	7.65	8.70	7.05	7.0	7.0	6.75	5.75	4.45	3.65	3.7	4.30
1.35	7.00	7.1	8.8	7.0	7.0	7.0	6.8	5.85	4.45	3.75	3.75	4.40
2.50	6.85	7.15	9.1	7.05	7.1	7.0	6.75	5.85	4.6	-	-	-
5.25	7.05	7.70	9.50	7.10	7.15	7.20	6.90	6.0	5.0	3.85	3.8	4.50

Table 3 Dielectric Parameter Obtained from Dielectric Dispersion and Cole-Cole plots for X-irradiated and non-Irradiated Rat Testis

Dose (mGy)	ε_s	ε_∞	$\Delta(\varepsilon_s - \varepsilon_\infty)$	F_R(Hz)	$\tau(\mu s)$	α
0	30.14	12.22	17.92	20	53	0.09
0.15	27.22	10.38	16.84	20	50	0.09
0.67	25.76	9.82	15.94	20	47	0.08
1.35	13.61	5.19	8.42	20	25	0.04
2.50	10.69	4.08	6.61	20	18	0.04
5.25	6.81	1.76	5.05	20	27	0.02

The results show a highly nonlinear degradation of dielectric properties in ionizing radiation as shown in Table 3. Low doses (0–0.67 mGy) lead to a slow decrease of permittivity values (ε_s, ε_∞) and dielectric strength Δ, but a threshold seems to be reached between 0.67 and 1.35 mGy, after which the properties collapse suddenly. Δ decreases from 15.94 to 8.42 in this interval, which is a sign of catastrophic damage of the polarizable structure of the material.

The relaxation time τ generally decreases with dose, but shows a remarkable anomaly at the highest dose (5.25 mGy) where it increases from 18 μs to 27 μs. This suggests a basic change in the dominant relaxation mechanism. It may be related to the formation of new and more stable defect complexes that impose higher energy barriers to reorientation [3][8]. Such non monotonic behavior in τ along with sharp drop in permittivity indicates that high dose radiation not only damages the structure but it is transformed to a new state having different dielectric properties.

The mathematical models of the effect of X-irradiation on rats' testis for dielectric decrement, relaxation time and spread parameter are given below;

Spread of Parameters

Rat Testis in the Range of 20 Hz to 20 kHz

y = -2E – 05x2 + 0.0015x + 0.0903

Testis exhibits the most pronounced frequency dependence with the highest baseline (c=0.0903; -2 x 10^{-5} quadratic term), indicating complex cellular architecture [5]. Biologically, the quadratic terms represent

ISSN No. 2321-2705 | DOI: 10.51244/IJRSI |Volume XIII Issue X October 2026

tissue-specific relaxation processes, microstructural heterogeneity and dynamics of bound water, while the linear terms are related to ionic mobility, membrane capacitance and extracellular matrix density [12].

Dielectric Decrement

Rat Testis at frequency range of 20 Hz to 20 kHz

$y = -0.0044x^2 + 0.2599x + 17.973$

The frequency dependence here is very dramatic for the testis (a=-0.0044). Biological importance is that ; quadratic terms measure bound water relaxation , membrane capacitance effects and structural heterogeneity [5] while linear terms measure ionic diffusion processes, counterion polarization and interface phenomena [2]. The testis responds with high frequency sensitivity. Quadratic coefficients are associated with tissue hydration.

Relaxation Time

Rat Testis at frequency range 20 Hz to 20 kHz

y = -0.0098x2 + 0.5466x + 53.285

The testis has a strong quadratic term (a = -0.0098) indicating frequency dependent tubule dynamics and a moderate baseline (c = 53.285) balancing cellular and fluid components [5]. The quadratic terms relate to biophysical meaning of microstructural heterogeneity, multiple relaxation processes and bound water transitions [2] and linear terms relate to ionic mobility constraints, membrane capacitance and extracellular matrix density [12]. The above mentioned quadratic formulas describe the frequency dependent behavior of dielectric spread parameters α in various rat tissues and exhibit important biophysical properties. All equations have the general form: $\alpha(f) = af2 + bf + c$ [14].

where f is the frequency (Hz), an is the curvature coefficient, b is the linear coefficient, c is the baseline spread parameter

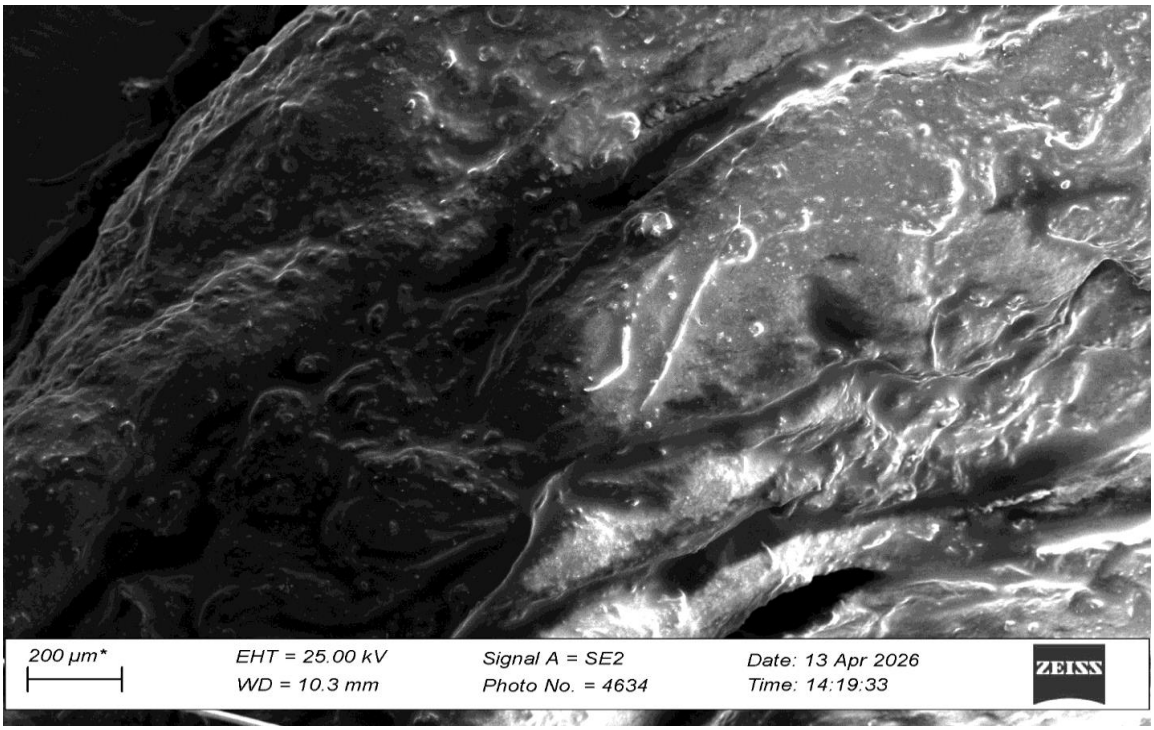


Figure 1: A SEM image of non-irradiated albino rats' testis tissue sample.

ISSN No. 2321-2705 | DOI: 10.51244/IJRSI |Volume XIII Issue X October 2026

Figure 1 shows a SEM image of a healthy testis tissue sample. The sample shows a large, continuous, multi-layered cell mass extending diagonally across the image. The surface is very cohesive so the tissue boundaries and structure are well preserved. This is typical of the healthy control state. The tissue is dense and there's not much crumbling or random shedding.

The right side of the tissue is smooth and shiny with gentle waves and broad ripples. This is the outer covering or connective sheath which is intact. No damage and pits have been developed. As we go left, the surface becomes more textured, granular and wavy. This area has fine wrinkles and nodular bumps. These folds collapse uniformly when dried in vacuum. This means the cells and spaces below are packed in tight and are stable.

There is a deep, organized groove that runs along the upper right and far left edges. The grooves create natural depth drops. Instead of fracturing irregularly, the tissue splits along neat, predictable boundaries.

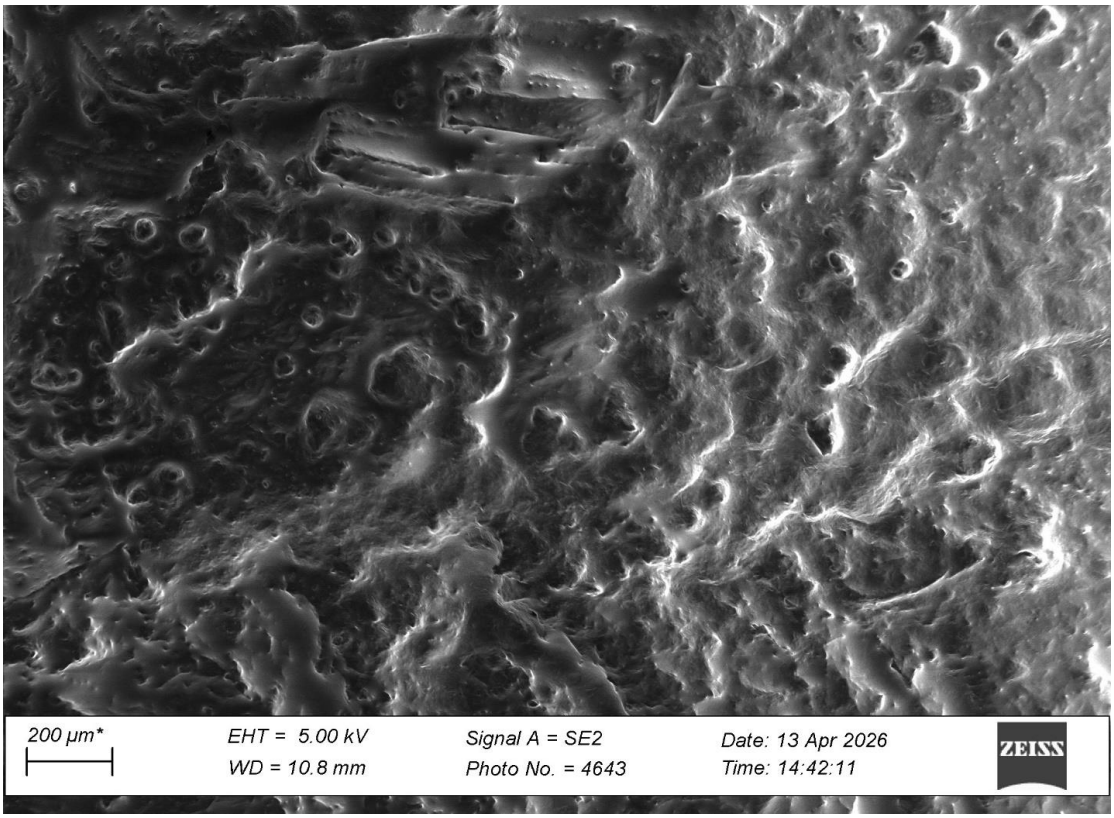


Figure 2: A SEM image of irradiated albino rats' testis tissue sample.

The micrograph in figure 2 showed large mass of dehydrated tissue and severe damage and erosion of surface of irradiated testis tissue. The main change is the presence of many tiny holes, pits and deep cavities scattered throughout the entire tissue. The smooth outer layer of healthy tissue is entirely missing. The surface is replaced by a porous, degraded surface that looks like a honeycomb sponge. This shows major breakdown of the tissue structure and of the boundaries of the cells. The long, thin multiple fibres could only be a testicular interstitial tissue with long fibrous structures on the surface. Sperm tails may be the ring/bend fibre. This means the supportive framework has cracked and come apart due to the radiation dose of 5.25 mGy. A major change is seen in comparing control and irradiated testis tissue; a transition from a cohesive, organized structure to a badly eroded, porous network. The control tissue is composed of a strong continuous multi-layered cell mass with smooth wavy surfaces and unbroken outer protective sheaths. It folds neatly under hoover into regular wrinkles, and tears only along smooth predictable cracks. This maintains the internal structure for high electrical charge storage.

This unified structure completely collapses in the irradiated tissue after 5.25 mGy. The smooth surface is replaced by a porous degraded landscape with many tiny holes, deep cavities and sharp rectangular gaps that form a honeycomb pattern. The underlying tissue is disintegrating, flaking and cracking – the basement

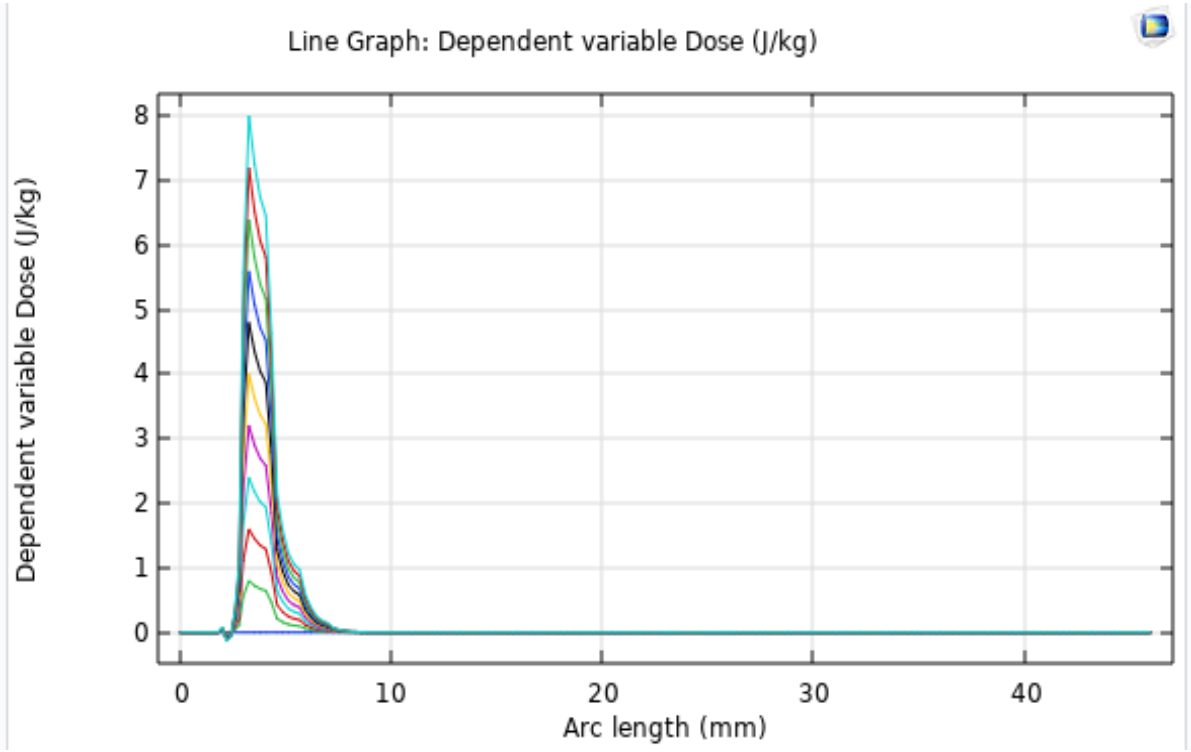
ISSN No. 2321-2705 | DOI: 10.51244/IJRSI |Volume XIII Issue X October 2026

membranes around the seminiferous tubules have catastrophically failed. This structural breakdown changes the electrical properties of the tissue. It holds less electrical charge (lower permittivity) due to the loss of cell boundaries and it conducts electricity more easily (higher conductivity) in the low frequency range (20 Hz to 20 kHz).

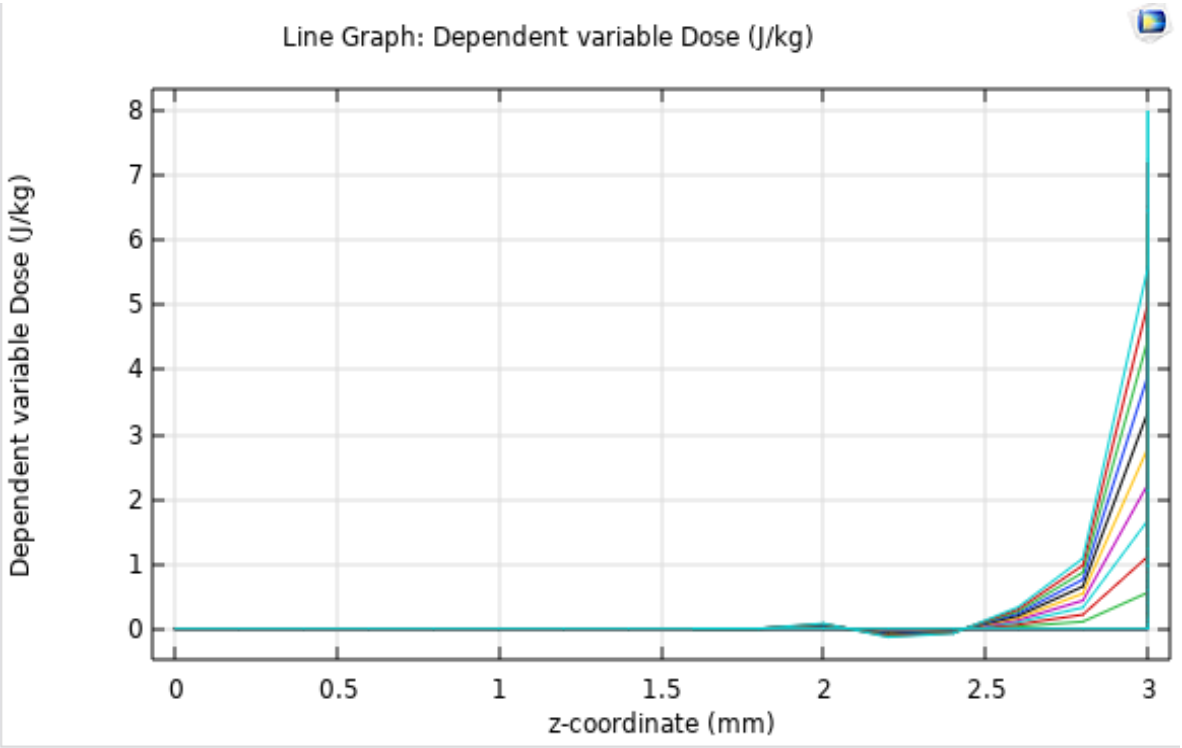
COMSOL Multiphysics Simulation

For numerical simulation of the X-ray attenuation and energy deposition in COMSOL Multiphysics, it is required to follow the high-energy radiation transport and local energy loss measures in the target domains. The numerical framework is constructed upon the governing physics of the Beer-Lambert law combined with fundamental atomic attenuation matrices to calculate spatial power deposition profiles and the subsequent conversion of electromagnetic energy to localized thermal or dosimetric fields. A 2D axisymmetric formulation in a 3D computational volume was used to evaluate spatial distribution, depth penetration dynamics and volumetric interactions of incident X-ray beam. This geometric optimization exploits angular symmetry to significantly cut down on computation overhead and degrees of freedom while preserving strict spatial accuracy along the main axis of beam propagation (the z-axis). The basic material properties were; absorption coefficient, electrical conductivity, and relative permittivity. The baseline geometry was represented as a solid cylindrical phantom so as to simulate multi-layered biological domains. The boundary system has orthogonal triad (t_1, t_2, n) which emanates from deformed configuration frame setting. The spatial global Cartesian (z-axis) is where the first tangent direction is created from.

A parametric sweep over a discrete continuum of photon energies (E) was performed to model a monochromatic spectral profile. Dynamic implementation of energy-dependent material properties was achieved by interpolating empirical mass attenuation coefficients (μ/ρ) corresponding to the changing incident photon spectrum into the computational domain. The intensity of the primary incident X-ray beam (I_0) was systematically parameterized with a structured indexing matrix directly correlated to the specific properties of the biological tissue constituents under investigation. A localized switch expression was used to create numerical segmentation to resolve spatial material transitions and structural boundaries across the phantom sub layers. The physical basis of the radiation transport and local energy deposition was provided by the mathematical physics interface. This provided a mapping of the absorbed dose (D quantified in J/kg) over the tissue geometry. The resulting attenuation gradients and depth dose profiles were post-processed and extracted along the central axis of propagation after the convergence of the parametric sweep.



ISSN No. 2321-2705 | DOI: 10.51244/IJRSI |Volume XIII Issue X October 2026



From the graphs above; the Y-axis shows the dependent variable Dose (J/kg), which represents the absorbed radiation dose (where 1 J/kg = 1 Gray (Gy)). The X-axis represents the arc length (mm) which represents the penetration depth or path length into the medium. The graph displays a sharp peak very close to the entrance surface (around an arc length of 1 to 3 mm), followed by a rapid, near exponential decay that drops close to zero as the path length extends past 10 mm.

The behaviour shown in this graphs is highly characteristic of x-rays passing through matter where photons hit the surface and immediately begin creating secondary electrons through processes like the photoelectric effect and Compton scattering. This leads to a rapid build up to a maximum dose very close to the interface (seen here around 2 mm). Also x-rays are uncharged particles and so interact probabilistically along their whole path. When they reach a maximum of ionization, their intensity decays exponentially, according to the Beer-Lambert Law ($I \alpha e^{(-\mu x)}$). This accounts for the long, smooth downward slope seen when arc length is from 3 mm up to over 10 mm. X-rays attenuate continuously and have theoretically infinite range. They continue to deposit dose all the way through the material until the beam is completely attenuated [18].

The COMSOL graph shows a standard x-ray depth dose distribution, where absorption is highest near the entry point and falls off gradually over depth. It illustrates how x-rays behave in contrast to charged particles, as it lacks the characteristically deep, clean maximum energy deposition zone defined by a Bragg Peak [16][17].

CONCLUSION

This work suggests that low-dose X-rays may affect albino rat testis biophysical and structural properties in a non-linear and threshold-dependent manner. This occurs in the 20 Hz-20 kHz low-frequency α-dispersion area. The structural and electrical characteristics remain essentially constant at low radiation exposures (0–0.67 mGy). Between 0.67 and 1.35 mGy, a biophysical threshold is reached. After this point, the tissue's polarized structure breaks down, resulting in a significant fall in dielectric strength (Δ), static permittivity (ε_s), and relaxation time (τ). Low frequency electrical conductivity (π) rises as cell borders break down and fluid-filled extracellular channels develop.

Looking at the structure using a SEM shows electrical changes. The microphotographs indicate that 5.25 mGy-exposed tissues changed from a solid multilayered cell mass to a badly damaged, porous, honeycomb-like architecture. This suggests the seminiferous tubule basement membranes were completely destroyed.

Additional 2D axisymmetric COMSOL Multiphysics simulations effectively mapped the spatial depth-dose distribution. According to the Beer-Lambert law, most energy was deposited around the entrance surface (1–3 mm) and then declined exponentially. Finally, the empirical quadratic formulas produced in this work can be used to simulate soft tissue electromagnetic interactions. These novel ideas can improve bioimpedance-based tracking algorithms for clinical radiotherapy planning and radiation safety.

Ethical Approval

An ethical clearance certificate was obtained for this research since it involved the use of laboratory rats through the Office of the Vice Chancellor, Director of Research and Creative Thoughts with reference FUL/DIRECT/ECC/2026/HU:0008.

Conflict of Interest Statement

The authors declare that the research was conducted in the absence of any commercial or financial relationships that could be construed as a potential conflict of interest.

REFERENCES

1. Bottiglieri, A., Sheth, R. A., & Prakash, P. (2023). A Computational Modeling Approach to Investigate the Influence of Hyperthermia on the Tumor Microenvironment. Journal of visualized experiments : JoVE, (202), 10.3791/65870. https://doi.org/10.3791/65870
2. Castro, R., Spivak, Y., Shevchenko, S., & Moshnikov, V. (2021). Low-Frequency Dielectric Relaxation in Structures Based on Macroporous Silicon with Meso-Macroporous Skin-Layer. *Materials*, *14*(10), 2471. https://doi.org/10.3390/ma 14102471
3. Chen, L. F., Ong, C. K., Neo, C. P., Varadan, V. V., & Varadan, V. K. (2023). Microwave electronics: Measurement and materials characterization (2nd ed.). Wiley-IEEE Press.
4. Cheng, Y., & Fu, M. (2018). Dielectric properties for non-invasive detection of normal, benign, and malignant breast tissues using microwave theories. Thoracic cancer, 9(4), 459–465. https://doi.org/10.1111/1759-7714.12605
5. Foster, K.R. (2008). Dielectric properties of biomaterials & biomedical engineering. 2nd Edition, CRC Press. 11. ISBN 9780429154065.
6. Fischer, E. R., Hansen, B. T., Nair, V., Hoyt, F. H., Schwartz, C. L., & Dorward, D. W. (2024). Scanning Electron Microscopy. Current protocols, 4(5), e1034. https://doi.org/10.1002/cpz1.1034
7. Gabriel, S., Lau, R. W., & Gabriel, C. (1996). The dielectric properties of biological tissues: II. Measurements in the frequency range 10 Hz to 20 GHz. Physics in medicine and biology, 41(11), 2251–2269. https://doi.org/10.1088/0031-9155/41/11/002.
8. Jonscher, A. K. (1999). Dielectric relaxation in solids. Journal of Physics D: Applied Physics, 32(14), R57–R70. https://doi.org/10.1088/0022-3727/32/14/201
9. McBride, W. H., & Schaue, D. (2020). Radiation-induced tissue damage and response. The Journal of pathology, 250(5), 647–655. https://doi.org/10.1002/path.5389
10. Orkaa, M. S., Bello, A. A., Dlama, J. Z., Ewuga, U. J. (2024) Evaluating the Dielectric Characteristics of Tissues: A Relationship Between Low Frequency Range and Dryness. Nigerian Journal of Physics 33(2): 146-156. https://doi.org/10.62292/njp.v33i2.2024.229
11. Pelletti, G., Martini, D., Ingrà, L., Mazzotti, M. C., Giorgetti, A., Falconi, M., & Fais, P. (2022). Morphological characterization using scanning electron microscopy of fly artifacts deposited by Calliphora vomitoria (Diptera: Calliphoridae) on household materials. International journal of legal medicine, 136(1), 357–364. https://doi.org/10.1007/s00414-021-02634-8
12. Peyman, A., Rezazadeh, A. A., & Gabriel, C. (2001). Changes in the dielectric properties of rat tissue as a function of age at microwave frequencies. Physics in medicine and biology, 46(6), 1617–1629. https://doi.org/10.1088/0031-9155/46/6/303
13. Sasaki K., E. Porter, E.A. Rashed, L. Farrugia and G. Schmid (2022). Measurement and image-based estimation of dielectric properties of biological tissues —past, present, and future. Phys. Med. Biol. 67 (2022) 14TR01 https://doi.org/10.1088/1361-6560/ac7b64

14. Sombo, T., Ige, T. A., & Agba, E. H. (2015). Mathematical Modelling of the Effects of Gamma Irradiation on Dielectric Dispersion of Bovine Liver Tissues at Low and Radiofrequency. 5(1), 12–17. https://doi.org/10.5923/j.biophysics.20150501.02
15. Wei W, Ren Y, Lan J, Yi J, Wang M, Zhang Y, Wang S, Xu Y, Han G, Fu Y, You L, Xue J, Jin S, Li J. (2026). Ionizing radiation: molecular mechanisms, biological effects, and therapeutic targets. Mol Biomed. 7(1); 3. doi: 10.1186/s43556-025-00358-4. PMID: 41507636; PMCID: PMC12783457.
16. Choi, W.H., & Cho, J. (2015) Evolving clinical cancer radiotherapy: concerns regarding normal tissue protection and quality assurance. J Korean Med Sci, 31, 75-87. http://dx.doi.org/10.3346/jkms2016.31.S1.S75
17. Desouky, O., & Zhou, G. (2015). Biophysical and radiobiological aspects of heavy charged particles. Journal of Taibah University for Science, 162, 1-8. http://dx.doi.org/10.1016/j.jtusci.2015.02.014
18. Berman, A.T., St. James, S., Rengan, R. (2015). Proton beam therapy for non-small cell lung cancer: current clinical evidence and future directions. Cancers,7, 1178-90; doi: 10.3390/cancers7030831